X-ray structure of polyaniline

5 AUTHORS, INCLUDING:

Jean-Paul POUGET
Université Paris-Sud 11

317 PUBLICATIONS   **6,125** CITATIONS

X-ray Structure of Polyaniline

J. P. Pouget*

Laboratoire de Physique des Solides, LA2 CNRS and LURE, Université Paris-Sud, 91405 Orsay, France

M. E. Józefowicz† and A. J. Epstein*

Department of Physics and Department of Chemistry, The Ohio State University, Columbus, Ohio 43210

X. Tang and A. G. MacDiarmid

Department of Chemistry, University of Pennsylvania, Philadelphia, Pennsylvania 19104

Received May 2, 1990; Revised Manuscript Received July 31, 1990

ABSTRACT: We distinguish between two classes of the emeraldine form of polyaniline. Class I emeraldine is that for which the conducting HCl salt exhibits ES-I crystal structure and the insulating base form is essentially amorphous EB-I. In general, class I materials are formed when the polymer is obtained from solution in the protonated form. Samples of polyaniline belonging to class II possess ES-II structure in the conducting HCl salt form and EB-II structure in the insulating base form. Emeraldine samples belonging to class II were prepared originally in the nonprotonated form. The crystalline components of ES-I, EB-II, and ES-II have been analyzed, and basic parameters of the structures have been derived from comparison between diffraction patterns and intensity calculations. EB-II has a structure similar to that of chemically analogous polymers such as poly(phenylene sulfide) and poly(phenylene oxide). ES-I and ES-II structures differ substantially in their compactness. In class I the increase of crystallite size and decrease in interchain separation with protonation correlate with increasing three-dimensional delocalization of charge with increasing protonation. In contrast, in partially crystalline EB-II, initially protonation occurs in amorphous regions with only subsequent doping into the crystalline areas.

1. Introduction

Conducting polymers have been of interest because of the electronic states as well as the high conductivities that occur upon doping.[1] The detailed lattice structure determines the electronic structure degeneracy and hence whether soliton,[2,3] polaron,[4] or bipolaron defects[5] occur upon light doping or photoexcitation. Extensive doping of polyacetylene leads to an evolution of the structure of the polymer so that at first charged solitons are stable and finally a metallic state is formed.[6-8] Studies of other conducting polymers have been hampered by the absence of detailed information on the local crystalline structure and its evolution with doping.

The insulating emeraldine base (EB) illustrated in Figure 1i differs from polymers studied earlier in several important aspects. First, its energy gap arises from the electronic structure of the constituent C_6 units in contrast to the role of bond length alternation (Peierls distortion) for polyacetylene, polythiophene, etc.[9-11] Second, also in contrast with polyacetylene and polythiophene, it is not charge conjugation symmetric.[11] Third, both carbon rings and nitrogen atoms are within the conjugation path, forming a generalized "A-B" polymer.[12] Fourth, the C_6 benzenoid rings of polyaniline can rotate or flip, significantly altering, by electron–phonon interaction, the electronic structure.[10,13] Fifth, EB can be converted from an insulating to a metallic state (ES) if protons are added to the $-N=$ sites while the number of electrons in the chain is held constant.[14,15] Earlier studies proposed[15-17] the formation of a metallic polaron lattice (with disorder) in ES (Figure 1ii). Partial protonation was proposed to lead to phase segregation between protonated and unprotonated regions.[15] These concepts were in agreement

† Chemical Physics Program, The Ohio State University, Columbus, Ohio 43210-1106.
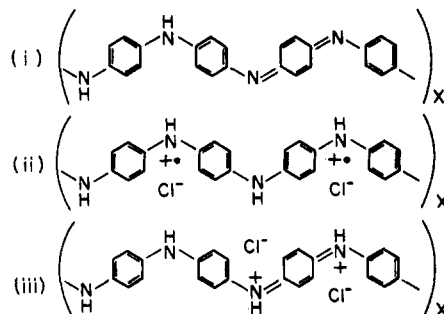
Figure 1. Schematic illustrations of polymer repeat units for (i) emeraldine base, (ii) polaron form of emeraldine salt, and (iii) bipolaron form of emeraldine salt.

with band structure[11] and lattice energy calculations,[17] optical,[11,15,18-20] and transport studies.[21,22] Later, it was proposed[23-25] that the protonated polymer was strongly disordered and formed a Fermi glass. In other works, the bipolaron state (Figure 1iii) was suggested[24,26] to be most important for the heavily doped compositions.

Very little is known on the structure of polyaniline. Baughmann et al.[27] investigated crystals of ClO_4^- and BF_4^- salts of "tetramers" and "dimers" of aniline. Recently, crystallinity in some polyaniline forms was reported[28,29] but the structural characteristics were not investigated in detail. The purpose of this paper is to present a consistent study of the crystallinity of the various forms of polyaniline together with the parameters of their structure. It completes our results briefly reported earlier.[30]

In accord with this earlier work, we report structures for two distinct classes of emeraldine. Class I emeraldine is that for which the base form is essentially amorphous EB-I and the HCl salt exhibits ES-I structure. In general, class I materials form when the polymer is obtained from solution in protonated form. Class II emeraldine is that

© 1991 American Chemical Society

for which the base exhibits partially crystalline EB-II structure and the HCl salt the ES-II structure. In general, class II materials are formed when the polymer is obtained from solution in the nonprotonated form or through treatment of EB-I with tetrahydrofuran (THF) and/or *N*-methyl-2-pyrrolidone (NMP). The variation of order in these polymers as a function of the protonation level is presented. The proposed EB-II crystal structure corresponds with that of our earlier work,[30] while new diffraction data has led to refinement of the earlier proposed ES-I and ES-II structures.

Section 2 details the preparation of the samples and the experimental conditions of the structural study. The results thus obtained are given in section 3, and the structures are analyzed in section 4 and discussed in section 5. Conclusions are summarized in section 6.

2. Experimental Section

The facile chemistry of polyaniline allows for several routes for synthesis and processing of materials. The relationship between synthesis and processing conditions and degree of crystallinity, coherence lengths, and detailed crystal structure is therefore of importance. Hence in this study we have undertaken the preparation of the different forms of emeraldine by various methods:

Polyaniline (emeraldine base and emeraldine salt powder) was made by our standard procedure.[31] Oxidant ($(NH_4)_2S_2O_8$) was added to the solution of aniline in 1 M HCl, and 42% protonated emeraldine hydrochloride ES-I powder precipitated. This powder was subsequently converted into emeraldine base EB-I form by washing it with 0.1 M NH_4OH solution. Alternatively, ES-I powder was synthesized at lower temperature (−13 °C) and was not converted to emeraldine base EB-I but treated with HCl to obtain a doping level of 50%. X-ray data obtained on this ES-I powder, named "**low-temperature**" **ES-I**, will serve as a basis of most structural evaluations on the ES-I structure in this paper.

Acid-cast film (emeraldine acetate) was prepared by dissolving emeraldine base powder in 80% acetic acid, casting the solution on a glass substrate, evaporating the solvent, and removing the film from the glass surface by immersing it in 2% aqueous HF. Films obtained in this way were subsequently washed with 0.1 M NH_4OH[32] to convert to the emeraldine base EB-I form.

Electrochemically prepared film of emeraldine hydrochloride (ES-I) was deposited on the Pt electrode by cycling the potential of the electrode from −0.15 to +0.75 V vs SCE in an aniline solution in 1 M HCl for 4 h.[33] The film was removed from the solution at a potential of ∼0.40 V, characteristic of the emeraldine oxidation state.

NMP-cast film (EB-II) was made by dissolving the polyaniline base powder in *N*-methyl-2-pyrrolidone (NMP). The solution was then cast on a glass substrate and dried in air in an oven at 70 °C for 16 h.[34] Some samples were then uniaxially oriented by stretching at ca. 110 °C in argon.[35]

DMSO-cast film (EB-II) was made by dissolving the polyaniline in dimethylsulfoxide (DMSO), casting the solution on a glass substrate, and drying in air in an oven for 16 h.

THF/NMP-extracted emeraldine base powder (EB-II) was prepared by extracting the emeraldine base powder (EB-I) with tetrahydrofuran (THF) until the liquid was colorless, then extracting with NMP until the liquid was almost colorless, and vacuum-drying for 48 h at room temperature.[36] The powder obtained has been confirmed by infrared measurements to be free from NMP.

THF extract was collected during the above extraction process and vacuum-dried. Black emeraldine base (EB-II) powder precipitated. It was shown[36] that extracted material has significantly lower molecular weight than emeraldine base powder prepared by standard procedure and is impure (total of % C + % H + % N = 97.02%).

All the emeraldine base samples were HCl-"doped" by equilibrating with HCl solutions of appropriate concentration. For class I samples the pH of the doping solution was measured and

the percent doping was obtained from the previously published doping level/pH curve.[37] The [Cl]/[N] ratio (i.e., doping level) of class II material obtained from the THF/NMP extraction was determined by elemental analysis. The pH dependence of the percent doping for this class II material is somewhat different from that of class I.[38]

As in earlier studies of polyacetylene[39] X-ray data were collected on photographic film fixed on a cylindrical camera with the sample placed in the center of the chamber and maintained under vacuum. X-ray patterns were taken with monochromatized Cu Kα (λ = 1.542 Å) radiation. Additional data were also obtained with the higher resolution X-ray synchrotron radiation (λ = 1.596 Å and λ = 1.551 Å) at the station D-16 at LURE (Orsay). X-ray films were read in the equatorial plane with a Joyce-Loeble microdensitometer.

3. Experimental Results

Depending on the method of preparation, we observe two different crystalline forms of the emeraldine base and its HCl salt, even though the chemical composition is the same in each case. As noted in the Introduction, these materials can be categorized as two different classes, I and II. Usual protonation/deprotonation procedures leave one consistently within a single class. There are procedures however that enable conversion of materials from one class to the other. Preparations of NMP-cast film, DMSO-cast film, and THF/NMP-extracted emeraldine base powder (section 2) are essentially methods for converting class I emeraldine base (EB-I) into class II emeraldine base (EB-II). The interconversion of class II material to class I can be accomplished by dissolving EB-II in NMP and precipitating class I emeraldine salt (ES-I) with gaseous HCl.

3.1. Class I Materials. Chemically and **electrochemically** synthesized emeraldine and **acid-cast emeraldine film** have essentially identical emeraldine base structure EB-I and emeraldine hydrochloride structure ES-I. These materials are labeled here class I. A typical Debye–Scherrer pattern of the hydrochloride salt form of the emeraldine powder ("low-temperature" material), labeled emeraldine salt I (ES-I), is shown in Figure 2B. It exhibits well-defined rings. The three materials mentioned above show the same structural features when in the HCl salt form, sometimes with slight differences in *d* spacings. Figure 3b is a microdensitometer tracing of a ES-I "low-temperature" powder (synthesized at −13 °C). The *d* spacings deduced from the angular position 2θ of the observed peaks, according to the Bragg formula

$$\lambda = 2d \sin \theta \qquad (1)$$

are given in Table I (λ is the X-ray wavelength used). The table also includes an estimate of the relative intensity of these rings. The rings are broader than the experimental resolution (Δ(2θ) ≈ 0.05°) from which it is concluded that the crystalline order is incomplete. The crystalline domain size or the extent of order, *L*, can be estimated from the rings' angular width Δ(2θ) (full width at half-maximum (fwhm)) using the Scherrer formula[40]

$$L = \frac{0.9\lambda}{\Delta(2\theta) \cos \theta} \qquad (2)$$

The *L* values, associated with the strongest rings, are given in Table I. Typically, *L* ranges from 30 to 70 Å. The microdensitometer reading of Figure 3b shows that the rings are in fact superimposed on a broad scattering centered at ca. 2θ ∼ 25°, which is associated with X-ray diffraction of amorphous regions in the sample (in the case of powder samples a significant contribution to this scattering is due to the Lindemann glass sample holder). The fraction crystallinity X_c, estimated by comparing the integrated intensity of the rings above the amorphous
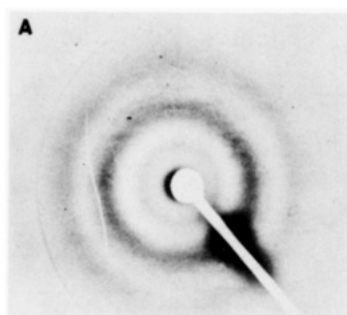
E B I
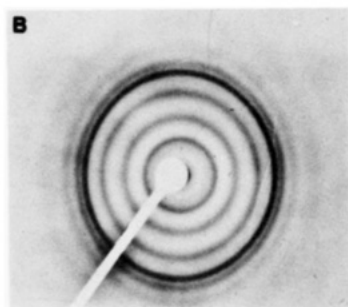
E S I (Cl/N ~ 0.5)

POLYANILINE POWDER

(λ = 1.596 Å)

Figure 2. X-ray Debye–Scherrer patterns from (A) EB-I and (B) "low-temperature" ES-I ($x \sim 0.5$) taken at LURE ($\lambda = 1.596$Å). The thin ring at large 2θ for EB-I is due to contamination with Al.

**Table I
Emeraldine "Low-Temperature" HCl Salt ES-I ([Cl]/[N] ~ 0.5): d Spacing, Domain Length L, and (hkl) Pseudoorthorhombic Indexation (From Figures 2b and 3b)**

d, Å	L, Å	intensity	$(hkl)^a$
9.57	45	s	(001)
5.94	35	s	(010)
4.26	35	s	(100)
3.51	70	vs	{(110)}
3.28	45	m	{(111)}
2.98	30	w	(020)
2.85		vw	{(112)}, {(021)}
2.47		w	{(120)}
2.34		vw	{(121)}, {(113)}
~2.10		vw and v broad	
~1.72		vw and v broad	

^{a} {(hkl)} means a set of reflections with permutation of the sign of the indicies (they are equivalent in an orthorhombic symmetry, but not in a triclinic one).

Figure 4. Set of microdensitometer readings of X-ray Debye–Scherrer patterns showing the continuous evolution from EB-I to ES-I as a function of the [Cl]/[N] ratio ($\lambda = 1.596$ Å). The various tracings are not scaled to each other.
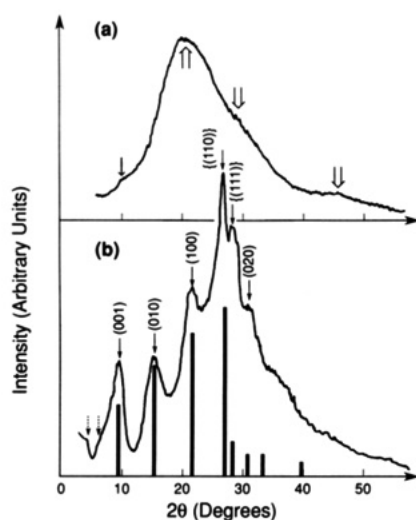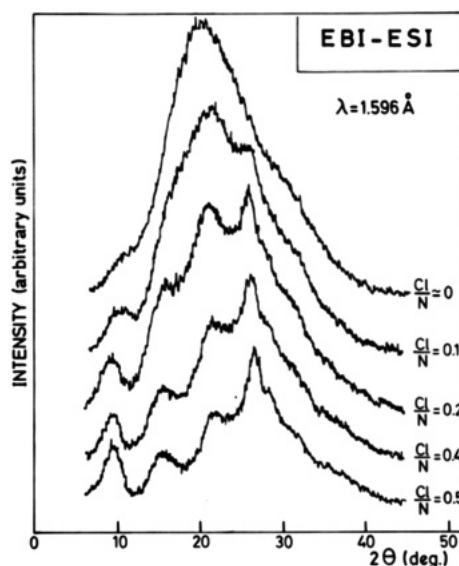

Figure 3. 2θ microdensitometer readings of the X-ray patterns from Figure 2. In EB-I (a) large arrows point toward the positions of the maxima of the broad, "amorphous" rings, and the thin arrow points toward the low-2θ reflection which is probably due to traces of ES-I. In ES-I (b) clearly visible rings are pointed at with arrows and some of them are indexed. Low-2θ additional features seen only for [Cl]/[N] $\sim$ 0.5 are shown by dotted arrows. The result of intensity calculations for the ES-I in the pseudoorthorhombic unit cell (see section 4.3) is presented as a bar diagram.

halo with the total scattered intensity (minus the Lindemann glass contribution), is approximately 50%.

The sharp rings of ES-I disappear upon compensation with NH$_4$OH. A typical X-ray pattern from the dedoped

material, termed emeraldine base I (EB-I), is shown in Figure 2A. A microdensitometer reading of this diffraction pattern is shown in Figure 3a. It consists mainly (double arrows) of one intense broad ring centered at ca. $2\theta \sim 20°$ ($d \sim 4.6$ Å), having a shoulder at ca. $2\theta \sim 30°$ ($d \sim 3$ Å), and of a weak ring at ca. $2\theta \sim 45°$ ($d \sim 2.1$ Å). These broad structures are characteristic of the diffraction by an amorphous polymer. The inner ring at ca. $2\theta \sim 10°$ (single arrow), very intense in ES-I (Figure 3b), is probably due to remaining traces of ES-I in the "dedoped" material.

EB-I when doped again with HCl becomes ES-I again, with a continuous evolution of its diffraction spectrum. This is more clearly illustrated by the microdensitometer readings shown in Figure 4 for different $x = $ [Cl]/[N] ratios (concentrations). A comparison between this figure and the microdensitometer reading from the "low-temperature" emeraldine salt (Figure 3b) shows that the low-temperature material corresponds to ca. $x \sim 0.5$. The evolution of the X-ray pattern for x increasing consists of (i) a gradual emergence of Debye–Scherrer rings from the EB-I amorphous halo together with a decrease of the amorphous content (the percent crystallinity roughly increases from near 0 at $x \sim 0$ to a maximum of ca. 50% at maximum doping level ($x = 0.5$)), (ii) a slight shift of the 2θ position of the Debye–Scherrer rings (this shift is
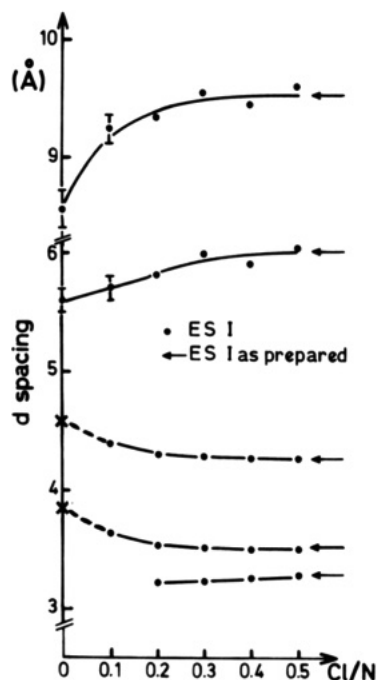
Figure 5. Variation of the d spacing of the strongest reflections of ES-I as a function of the doping level ([Cl]/[N] ratio). Arrows indicate the d spacing of "low-temperature" ES-I material. (×) gives d spacings of 4.6 and 3.8 Å observed in EB-II.
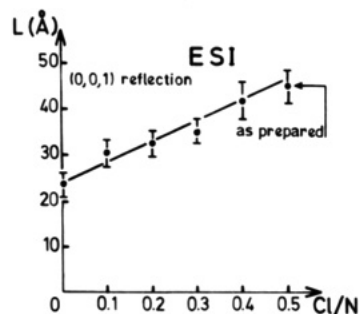

Figure 6. In-chain crystalline domain length, L, deduced from the width of the (001) reflection as a function of the [Cl]/[N] ratio for ES-I.

E B II

E S II (Cl/N ~ 0.5)

POLYANILINE NMP CAST FILM

($\lambda = 1.551$ Å)

Figure 7. X-ray patterns from stretched NMP-cast polyaniline films: (A) base EB-II and (B) salt ([Cl]/[N] ~ 0.5) ES-II data taken at LURE ($\lambda = 1.551$ Å). Stretching direction is indicated. Stretching ratio $l/l_0 = 3$.

more clearly expressed in Figure 5 in terms of d spacings, according to eq 1 (this figure includes also the data obtained from the "low-temperature" material (arrows)); for $x = 0$ the d spacings of ca. 8.6 and 5.7 Å correspond to what we suggest are the remaining traces of ES-I structure in EB-I—a similar shift in d spacings has been reported for H_2SO_4 protonated emeraldine[29]), and (iii) a sharpening of the rings, indicating an increase of the crystalline domain size L with x (only the quantitative evolution of L associated with the inner ring ($2\theta \sim 10°$ i.e., $d \sim 9$ Å) can be measured (see Figure 6)).

3.2. Class II Materials. Emeraldine films cast from NMP and DMSO solutions, THF/NMP-extracted emeraldine base powder, and THF-extracted low molecular weight emeraldine base powder all belong to a class of materials, labeled here as class II, that show significant differences with the class I materials, including (i) a crystalline emeraldine base structure (EB-II below) and (ii) upon doping of EB-II with HCl, a crystalline structure (ES-II) that differs from that of ES-I.[60]

A typical X-ray pattern from a threefold stretched NMP-cast (base) film is shown in Figure 7A. It shows a high degree of orientation, as deduced from several reflections having an arc of $\sim 20°$. These data allow a clear distinction between the in-chain, equatorial, and mixed reciprocal

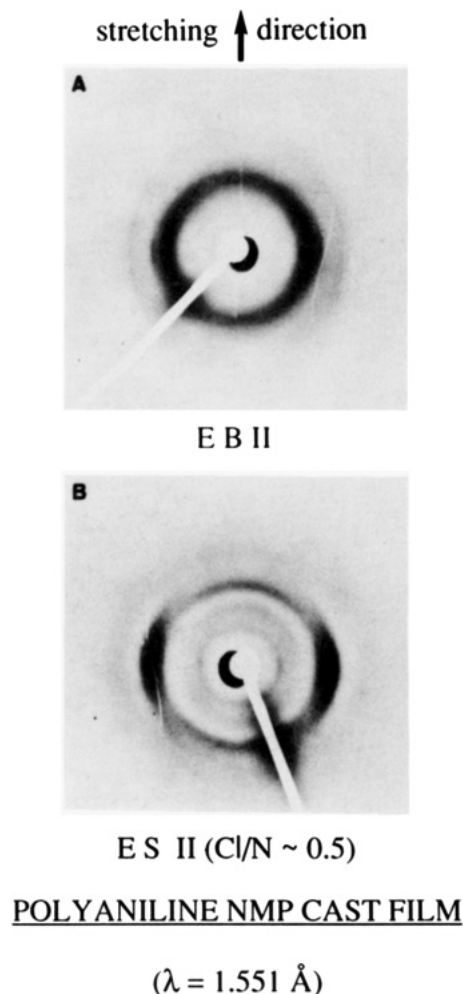directions. This is used in section 4 for indexation of X-ray patterns. The same reflections are also observed in THF-extracted polyaniline base powder (Figure 8a).

d spacings obtained from the 2θ positions of the reflections observed in these class II materials are collected in Table II. As in Table I, it includes an estimate of the relative intensity of the reflections, together with the crystalline domain length, L, deduced from the width of the strongest reflections. In particular, the crystalline coherence length measured in the polymer chain direction ($L_\parallel \sim 150$ Å) is ca. 3 times longer than that measured in transverse directions ($L_\perp \sim 50$ Å). The fraction crystallinity estimated for EB-II powder is ca. 50%.

The clear difference between the EB-I and EB-II materials concerns their crystallinity. In order to elucidate the structural relationship between EB-I and EB-II, we have studied the material obtained via the extraction of EB-I powder with THF. The part soluble in THF was collected, the solvent evaporated, and a Debye–Scherrer spectrum of the precipitated powder recorded. Its microdensitometer reading is shown in Figure 9a. It shows rings at the same d spacings as the THF/NMP-extracted powder (Table II). The rings are however sharper. From their width one concludes that the crystalline domain size has increased by a factor of 2. The Debye–Scherrer spectrum of the part of the emeraldine base powder insoluble in THF has also been recorded. The microdensitometer reading (Figure 9b) shows this insoluble part
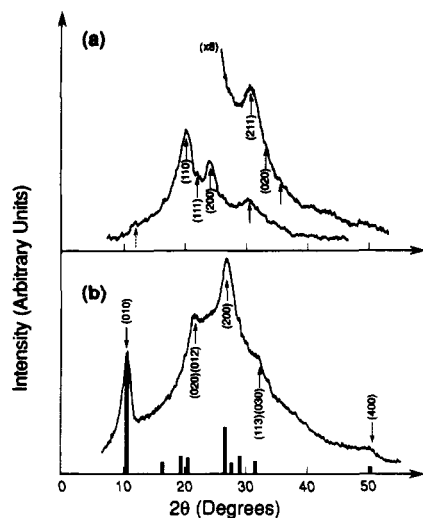
Figure 8. 2θ microdensitometer readings of powder Debye–Scherrer patterns from (a) EB-II and (b) ES-II taken at $\lambda = 1.596$ Å. Main rings are shown by arrows together with, for some of them, their indexation according to the $Pbcn$ and $Pc2a$ space groups, respectively. In (a) the dashed arrow points to an additional scattering seen on powder only. In (b) the bar diagram represents the result of intensity calculations for the ES-II in the $Pc2a$ structure.

to reflect the EB-II structure though with lower coherence length and crystallinity. One observes in its spectrum the onset of the main Debye–Scherrer reflections of EB-II. Approximate values of these d spacings are also given by Table II.

THF/NMP-extracted EB-II powder when doped with HCl retains its structure up to ca. $x \sim 0.25$. At this concentration a new structure, labeled ES-II below, appears. The ES-II structures coexist for $x = 0.25$. Only the ES-II structure is observed for $x = 0.4$ and $x = 0.5$. Figure 7B shows an X-ray pattern from a stretched and HCl-doped NMP-cast film ($x = 0.5$). Its degree of orientation is lower than that of the same film before doping (reflections having an arc of ca. 40°). The relative intensity and position of the reflections show striking differences from those of ES-I. The difference between the ES-I and ES-II crystalline structures is more quantitatively illustrated by a comparison between the microdensitometer readings from an ES-II ($x = 0.5$, Figure 8b) and an ES-I ($x = 0.5$, Figure 3b) powder pattern. The d spacing, relative intensity of the reflections, and crystalline domain length associated with some reflections for the ES-II powder and film are given in Table III. This table shows differences in the intensity and d spacings of the reflections observed in the powders and the films. Also the crystalline domain length, L, is greater by a factor of 2 in the powder ($\sim$50 Å) than in the film ($\sim$25 Å). However, the overall similarity of the diffraction patterns shows that the powder and the film have basically the same structural arrangement. The fraction crystallinity of ES-II is comparable to that of the starting base material EB-II.

EB-II when dedoped becomes amorphous.[30] Its X-ray pattern consists only of a broad and intense ring centered at ca. $d \sim 4.5$ Å. However, when doped again with HCl, amorphous EB-II becomes ES-II, not ES-I. This demonstrates that the two amorphous phases EB-I and EB-II have local structural differences. In this respect emeraldine exhibits an interesting "memory effect": upon doping it "remembers" the (base) state from which it was prepared.

4. Analysis of the Crystalline Structures

We begin with class II materials, for which the inspection of the diffraction patterns from oriented films (Figure 7) allows an indexation of the reflections with respect to the stretching (polymer chain) direction.

4.1. EB-II. The d spacings of the Bragg reflections observed from EB-II X-ray diffraction patterns are compatible with an orthorhombic lattice symmetry. Table II presents an indexation of the reflections of longest d spacing for this lattice symmetry. The lattice parameters have been obtained from a least-squares fit of the 2θ positions of those reflections having a single (hkl) contribution. The orthorhombic parameters found are as follows: $a = 7.80$ Å, $b = 5.75$ Å, $c = 10.05$ Å, and $V = 450$ Å^3 for the NMP-cast stretched film; $a = 7.65$ Å, $b = 5.75$ Å, $c = 10.20$ Å, and $V = 445$ Å^3 for the THF/NMP-extracted powder; $a = 7.65$ Å, $b = 5.65$ Å, $c = 10.40$ Å, and $V = 450$ Å^3 for the powder obtained from the THF-extracted solution.

The polymer parameter c varies appreciably among the different materials investigated. The value given corresponds to a zigzag repeat unit containing two rings. If the polymer contains an ordered sequence of benzenoid and quinoid rings as shown by Figure 1i, the actual periodicity must be $2c$. However, the subtle differences in the C–C and N–C distances between these two sequences and the linking of H to the N atoms terminating the benzenoid sequence can barely be detected by X-rays.

If an N–ring–N length of 5.52 Å[27] is taken, one obtains from the above-quoted parameters a ring–N–ring angle δ (defined in Figure 10a) ranging from 131° ($c = 10.05$ Å) to 141° ($c = 10.40$ Å). The former value agrees with that deduced from the X-ray refinement of ClO_4^- and BF_4^- salts of "tetramers" of aniline.[27] In fact, as stated above, the angle δ thus calculated can be considered only as an average angle of the polymer zigzag backbone.

Because of the limited number of reflections observed, the determinations of the orthorhombic space group of EB-II cannot be performed directly from the diffraction spectrum alone. However, it has been previously determined that the poly(p-phenylene sulfide) (PPS)[41] and poly-(p-phenylene oxide) (PPO)[42] composed also of X–ring–X (X = S or O instead of N and N–H for the emeraldine) zigzag polymer chains crystallize in the $Pbcn$ orthorhombic space group with lattice parameters very close to that of the polyaniline. The indices of the reflections allowed by the $Pbcn$ space group[43] are compatible with those quoted in Table II (the only exception concerns the (100) shoulder, which will be discussed below). Furthermore, the intensities estimated in Table II follow approximately those measured in PPS and PPO.[41,42] A schematic drawing of the EB-II structure in accord with the $Pbcn$ orthorhombic symmetry elements is given in Figure 10. As stated above, the $Pbcn$ space group holds if one neglects the difference between the benzenoid and quinoid sequences of the emeraldine chain and the hydrogen atoms bonded to amine nitrogens. Thus the $Pbcn$ space group describes either only the polymer backbone array of the polyaniline base if there is order between the benzenoid and quinoid sequences or an average structure if these sequences are disordered. It is noted that NMR studies support that the amine (i.e., C_6H_4–NH–C_6H_4–NH–) and imine (i.e., C_6H_4–N=C_6H_4=N–) alternate,[44] with the presence of excess imine due to handling of samples in the air.[45]

In order to quantitatively check this structure we have calculated the X-ray powder pattern with polyaniline chains located in the orthorhombic unit cell according to the above model. We made no distinction between qui-

<div align="center">

Table II
Emeraldine Base EB-II: *d* Spacing, Domain Length *L*, Intensity, and (*hkl*) Indexation

</div>

emeraldine base powder								
part insoluble in THF (from Figure 9b)	part soluble in THF (from Figure 9a)		THF/NMP-extracted powder (from Figure 8a)		NMP-cast stretched film (from Figure 7A)			
d, Å	*d*, Å	*L*, Å	*d*, Å	*L*, Å	*d*, Å	*L*, Å	intensity	(*hkl*)
					5.00	150	w	(002)
~4.57	4.56	100	4.57	50	4.60		vs	(110)
~4.25			4.20		4.27		vw	(111)
~3.82	3.83	100	3.82	50	3.91	50	s	(200)
~3.57	3.41		3.41				vw	(112)
~3.03	3.02	70	3.03	35	3.06		m	(211)
	2.82		~2.84		2.88		w	(020)
	~2.70		2.62				vw	(212)
	~2.48						vw	(121)
	2.33		~2.32				w	(213), (310)
~2.14	2.19		~2.21				w	(114), (221)
	1.95		~1.90				w	(024)
	1.84		~1.85				w	(321), (115), (130)

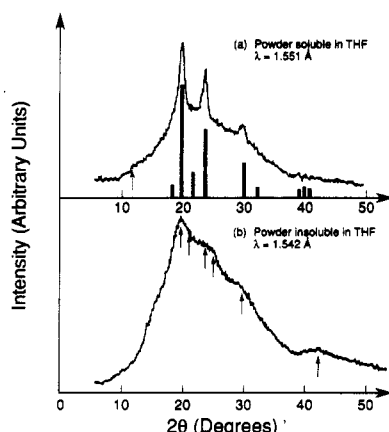**Figure 9.** 2θ microdensitometer readings of powder Debye–Scherrer spectrum from emeraldine base: (a) material extracted with THF from EB-I (λ = 1.551 Å); (b) part of EB-I not soluble in THF (λ = 1.542 Å). In (a) results of the intensity calculations are presented.

<div align="center">

Table III
Emeraldine HCl Salt ES-II ([Cl]/[N] ~ 0.5): *d* Spacing, Domain Length *L*, Intensity *I*, and (*hkl*) Indexation

</div>

powder (from Figure 8b)			stretched films (from Figure 7B)			
d, Å	*L*, Å	*I*	*d*, Å	*L*, Å	*I*	(*hkl*)
8.66	55	s	7.88	25	m	(010)
			5.87	20	m	(101)
4.32	55	m	4.38		w	(012)
			4.18		w	(102)
3.96		vw	3.96		vw	(020), (021)?
3.49	45	s	3.57		s	(200)
~3.23		vw	3.24		w	(210)
2.90		w				(113), (030)
~2.57		vw				(131), (123)
~2.44		vw				(014), (222)
~2.21		vw				(230), (311)
~1.90		vw				(034), (313)
~1.74		w				(400)

noid and benzenoid units. Bond lengths were assumed to be C–C = 1.41 Å, C–N = 1.36 Å, and C–H = 1.08 Å, based on oligomer values from ref. 27. The only parameter that is variable in this model is ring tilt angle ϕ (angle between each C_6 ring plane and the plane defined by the nitrogen atom positions). It is assumed that the angles ϕ alternate in sign for adjacent rings along a chain to minimize steric repulsion between neighboring C_6 rings.[10] The calculated relative intensities of the most intense reflections normalized to the strongest reflection are shown on Figure
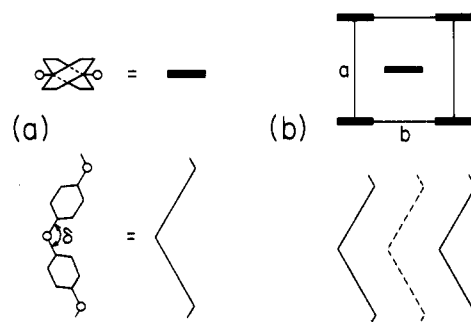

Figure 10. Projection along the chain axis and side view of the average structure of (a) the polyaniline chain and (b) EB-II. The dashed line represents a chain $a/2$ below or above the plane of the paper.
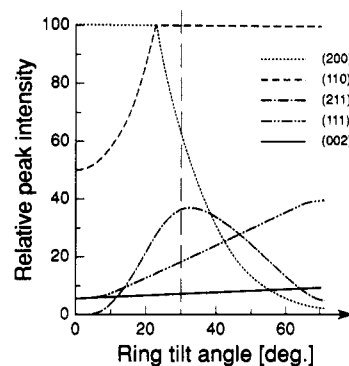

Figure 11. Calculated variation of the relative intensity of the five strongest reflections in EB-II as a function of the ring tilt angle ϕ, normalized to the most intense reflection. Vertical, dashed line represents the best fit to the experimental data at $\phi = 30°$.

11. The relative intensities of the (110) and (200) reflections depend strongly on ϕ, as shown on Figure 11. We have found that our calculated pattern agrees best with the experimental one for $\phi \sim 30°$. Angle $\phi \sim 30°$ compares with $\phi \sim 45°$ obtained from the structural refinement of PPS and PPO.[41,42] A comparison between experimental and calculated pattern is shown in Figure 9a. Calculated reflections with largest intensities are experimentally observed (their (*hkl*) indices are given in the last column of Table II).

Direct examination of the X-ray films for several powder samples (but not for polyaniline film samples) shows a weak shoulder centered at approximately the position of the (100) reflection ($d \sim 7.7$ Å) (dotted arrow in Figure 8a and 9a). Note that though these diffraction features are difficult to observe in the densitometer tracings, they

are clear in the original films. This reflection is asymmetric in shape and exhibits a long tail of scattering toward the large values of 2θ. Most likely, it corresponds to a Debye–Scherrer diffraction from a $(1kl)$ diffuse sheet or a diffuse rod located in this reciprocal plane. It can be associated with a correlated disorder breaking the $a/2$ translational symmetry of the structure projected on the a direction, possibly brought about by a defect in the relative ring tilt angle between two near-neighbor chains; hence it may reflect defects breaking the n-glide plane symmetry.

4.2. ES-II. The d spacings of the Bragg reflections observed from ES-II X-ray diffraction patterns are also compatible with an orthorhombic lattice symmetry. The indexation for the reflections of largest d spacing is given in Table III. A least-squares fit of their 2θ angular positions leads to the following orthorhombic parameters: $a = 7.1$ Å, $b = 7.9$ Å, $c = 10.4$ Å, and $V = 585$ Å^3 for the NMP-cast stretched film $(x = 0.5)$; $a = 7.0$ Å, $b = 8.6$ Å, $c = 10.4$ Å, and $V = 620$ Å^3 for the THF/NMP-extracted powder $(x = 0.5)$.

There is a large difference of b parameter between the two materials investigated. Differences in b parameters are also observed between different parts of the same powder. This prevents any determination of the evolution of the lattice parameters as a function of the [Cl]/[N] ratio. From the c (polymer chain) parameter we deduced, assuming an N–ring–N length of 5.52 Å, a ring–N–ring angle δ close to 141°.

With the small number of reflections observed it is difficult to derive the structure of ES-II directly. Since the volume of the ES-II cell is only 30% greater than that of EB-II, it should contain similarly two polymer chains per unit cell. (The excess volume of ca. 150 Å^3 is however 3 times larger than the volume of 2 × Cl$^-$!). The absence of the (100) reflection shows that the structure projected along the a axis has an $a/2$ translational symmetry. This is not the case in the b direction, since the (010) reflection is allowed. Although the reflections in the polymer chain direction are difficult to observe, one can assume from the absence of a strong (001) reflection that the structure projected along c still possesses the $c/2$ translational symmetry. Two orthorhombic space groups of maximal symmetry compatible with extinctions mentioned above are $P2_122_1$ and $Pc2a$. The most likely placement of the nitrogen atoms (with the constraint of 4 N per unit cell) is, as in the EB-II structure, to form an N backbone in the (b,c) plane.[43] As the unit cell must also accommodate 2 times less Cl atoms than N atoms (for $x = 0.5$), the Cl must also belong to a special position of the unit cell. The more likely possibility compatible with the large increase of the parameter b from EB-II to ES-II is to place the Cl on the twofold axis b, in the hollow of the polymer zigzag.

Two arrays considered, $P2_122_1$ and $Pc2a$, are shown in parts a and b of Figure 12, respectively (the first one was previously shown in Figure 4d of ref[30]). In $P2_122_1$ the polymer zigzags are in phase, while they are out of phase in $Pc2a$. In $P2_122_1$, the middle chain position along the b axis is not fixed by symmetry, $P2_122_1$ is a subgroup of $Pbcn$, which is not the case for $Pc2a$.

Calculations were made for theoretical powder patterns in both the $P2_122_1$ and $Pc2a$ structures, similarly as for EB-II. There are three variable parameters in the first structure: middle-chain shift u, Cl–N distance d, and ring tilt angle ϕ. In the second structure, only the Cl–N distance d and the angle ϕ can vary. In $P2_122_1$ a strong (110) reflection not observed experimentally is obtained unless a large shift of the middle chain (close to $b/2$) is introduced. The (110) reflection is not allowed in $Pc2a$.[43] In addition,
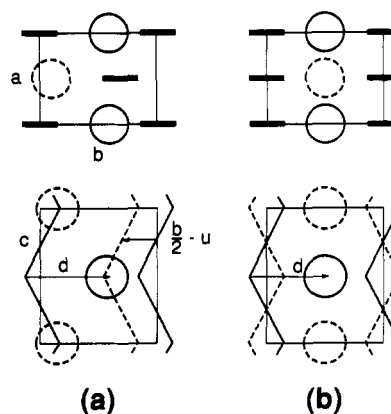

Figure 12. Projection along the chain axis and side view of the two orthorhombic structures considered for ES-II: (a) $P2_122_1$; (b) $Pc2a$.

the out-of-phase order of polymer chains along the a direction of a $Pc2a$ structure leads to lower interchain interaction than the in-phase order in $P2_122_1$ with large middle-chain shift. Model calculations show that the experimental data can be well accounted for by the $Pc2a$ structure. The relative intensities of the (010) and (200) reflections are very sensitive to the ring tilt angle ϕ and to the Cl–N distance d. The best agreement between the experimental and calculated spectra is obtained with $\phi = 0$–10° and $d = 5$–6 Å. Figure 8b compares the experimental and calculated $(\phi = 0°, d = 5$ Å$)$ spectra. The (101) and (111) reflections belong to the long tail of scattering between about $2\theta = 15°$ and 20°, where they cannot be resolved (a very weak (002) in-chain reflection is calculated). Table III gives indices of the more intense (hkl) reflections obtained by the calculation. They correspond to d spacings of reflections observed experimentally.

Angle ϕ close to zero means that rings lie nearly in the N backbone plane. This corresponds well with the tilt angle $\phi \sim 15°$ obtained from the structural refinement of ClO$_4$ and BF$_4^-$ salts of "phenyl-capped" tetramers of polyaniline.[27] The Cl–N distance found $(d \sim 5$–6 Å$)$ is about that expected for a compact packing of phenyl rings and Cl$^-$ in the hollow of the polymer zigzag. The $(b - d)$ distance, of about 3 Å, is also very close to the sum of the van der Waals radii of NH$_4^+$ (1.5 Å) and Cl$^-$ (1.8 Å) units.[46] In agreement with the low value of ϕ, the parameter a of ES-II is also very close to twice the van der Waals thickness of the phenyl ring, i.e., 2 × 3.35 Å.[46] In the film of ES-II studied, the large reduction of b and the slight increase of a could be accounted for by a slight increase of the ring tilt angle ϕ. The compactness of this structure along the a direction (compared with EB-II) makes ring rotations in ES-II difficult.

The $Pc2a$ structure is composed of layers of polymer chains alternating along b with layers of the Cl$^-$. Polymer chains are perpendicular to the (a,b) plane. Two successive chains along a have their zigzag backbone out of phase. Starting from the EB-II structure, the ES-II structure can be obtained by a relative shift of the middle chain by $\vec{b}/2 + \vec{c}/2$ and insertion of the Cl$^-$ between (a,c) layers. Because of the reconstructive nature of the doping process, it can be understood that dedoping of ES-II does not give back "crystalline" EB-II but leads to an amorphous material.

4.3. ES-I. In the absence of data from stretched films, the indexation of the reflections from the crystalline part of ES-I is more difficult to obtain. The d spacings measured from ES-I "low-temperature" powder $(x \sim 0.5)$ are given in Table I, and the evolution of some d spacings with the [Cl]/[N] ratio is shown on Figure 5.
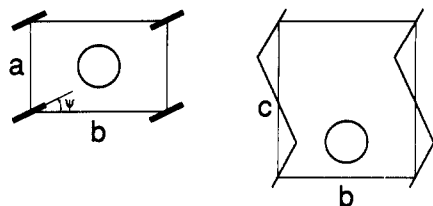
Figure 13. Projection along the chain axis and side view of ES-I.

We consider first the d spacings of the four strongest reflections: 9.6, 5.9, 4.26, and 3.51 Å. The largest d spacing is close to a polymer repeat distance. Thus it can correspond to the (001) reflection if, as before, we take c as a polymer repeat periodicity. However, the decrease of this d spacing from 9.6 Å (for $x \sim 0.5$) to ca. 8.6 Å ($x \sim 0$) suggests that the chains can be tilted with respect to the (a,b) basal plane, with an angle that decreases upon dedoping. The three other d spacings are close to the b, $ab/(a^2 + b^2)^{1/2}$ (i.e., d_{110}), and $a/2$ distances of EB-II, respectively, and they approach these EB-II values upon dedoping (Figure 5). This suggests that they correspond to the transverse (interchain) distances. Such an assignment is in agreement with an independent result[29] obtained from oriented fibers.

All the main reflections observed in the "low-temperature" ES-I (Table I) can be indexed in a pseudoorthorhombic cell[47] with lattice parameters $a = 4.3$ Å, $b = 5.9$ Å, $c = 9.6$ Å, and $V = 245$ Å^3.

The volume V thus obtained is slightly larger than that of an emeraldine base chain repeat unit (225 Å^3 or half the volume of the EB-II cell); the difference in volumes is close to the ionic volume of a Cl$^-$ anion ($\sim$25 Å^3). The ES-I unit cell contains a single polymer zigzag and a Cl$^-$ anion in very compact packing. Its volume per chain repeat unit is significantly smaller than that of the ES-II structure ($\sim$300 Å^3). The chain tilt observed upon dedoping means that either the true ES-I lattice symmetry is monoclinic with a or b as the unique axis or, more likely, triclinic, because of the absence of a twofold axis or mirror symmetry along a or b (see below). The value of the pseudo-orthorhombic c parameter for $x \sim 0.5$ leads to a ring–N–ring angle δ close to 120°.

The observation of two strong reflections of d spacings of 4.26 and 3.51 Å ((100) and (110) reflections, respectively) means that the packing of the near-neighbor chains is very similar in ES-I and EB-II. It is shown on the left side of Figure 13. The ES-I structure can be easily derived from EB-II by the insertion of a Cl$^-$ anion in the channel delimited by four adjacent chains. A very compact structure is obtained by assuming the placement of Cl$^-$ anions in the hollow of the polymer zigzag (Figure 13, right side). In principle, the sense of the triclinic deformation will depend on which hollow in the polymer zigzag is chosen for the insertion of the Cl$^-$.

We have calculated the Debye–Scherrer pattern for such a structure assuming that (i) the lattice is pseudo-orthorhombic, (ii) the bond lengths are identical with those used previously, and (iii) the Cl$^-$ is positioned in the plane of the nitrogens (parallel to the (a,b) plane) with distances to two neighboring nitrogens equal to 3.5 Å, which is approximately the sum of the N–H bond length and of the Cl$^-$ ionic radius.

This model contains two variable parameters: the ring tilt angle ϕ and the polymer chain setting angle ψ (defined in Figure 13). The calculated pattern contains the four previously discussed strongest reflections and agrees best with the experimental results for $\phi \sim 0–15°$ and $\Psi \sim$

20–30°. Figure 3b compares more quantitatively the experimental powder pattern and the calculated intensities for $\phi = 0°$ and $\Psi = 20°$, for which there is the best agreement. The indexation of the strongest reflections is given in the last column of Table I.

Although the structure proposed accounts for the position and intensity of the observed reflections, the X-ray pattern of salts with $x \sim 0.5$ (Figure 2B) shows additional features at small 2θ angles in the form of a shoulder on the low-2θ side of the (100) reflection, at a d spacing of ca. 13 Å, and in the form of a *central* scattering of external radius of ca. 19 Å (dotted arrows in Figure 3b). The understanding of these features, which are clearly present on the original X-ray films, needs further study, especially with small-angle scattering. These features, observed only in the heavily doped samples, are likely related to the Cl$^-$ anions. They can be caused by some inhomogeneity in the distribution of Cl$^-$ anions in the polymer.

5. Discussion

During the study we have obtained crystalline emeraldine base EB-II only through a recrystallization of amorphous EB-I. As the ES-I structure can be thought of as obtained by the insertion of Cl$^-$ anions into the channels of the EB-II structure, it is likely that, after dedoping, the polymer chains retain in amorphous EB-I a local order similar to that they adopt in crystalline EB-II. Further direct evidence is that EB-I powder when washed with THF shows broad reflections at about the same d spacings as that of EB-II (Figure 9b and Table I). More quantitatively, the X-ray powder spectrum shows a gradual increase of crystallinity along the sequence EB-I (Figure 3a), EB-I washed with THF (Figure 9b), EB-II (Figure 8a), and THF-extracted emeraldine base (Figure 9a). This implies that locally neighboring polymer chains are in phase in EB-I. In ES-II they are out of phase, and this ordering is likely kept on a local scale upon dedoping of ES-II into the amorphous EB-II. This difference of local order in amorphous EB-I and EB-II may explain the memory effect when doped EB-I goes to ES-I and doped EB-II (amorphous) to ES-II.

We now discuss the different "crystalline" structures of polyaniline. The EB-II structure is identical (ignoring the difference between benzenoid and quinoid rings and between imine and amine sites) with that of closely structurally related polymers: poly(p-phenylene sulfide) (PPS)[41] and poly(p-phenylene oxide) (PPO),[42] where N and N–H atoms of polyaniline are replaced by sulfur and oxygen, respectively. This supports that the *Pbcn* structural type is stabilized by van der Waals forces and by repulsions between the rings' π orbitals.

That two structures of emeraldine salts of quite different volumes are formed is at first glance surprising. However, the most compact structure, ES-I, is obtained by direct preparation (synthesis/precipitation of a salt form), while the less compact ES-II is obtained by converting crystalline EB-II into a salt form (i.e., by insertion of Cl$^-$ anions into a preexisting crystalline structure). To some extent, in the ES-I case, the insertion of Cl$^-$ into the channels of the polymer array resembles doping of polyacetylene with alkali metals,[48] while doping of EB-II (where ions are inserted between layers of polymer chains) recalls doping of polyacetylene with iodine.[6] In ES-I the neighboring columns of chlorine ions are in phase (i.e., Cl$^-$'s are at the same level), while in ES-II they are out of phase in the a direction (they are shifted by $c/2$). This could be due to the fact that direct Coulomb interactions between Cl$^-$ columns are effectively screened by the inbetween polymer

chains in ES-I (Figure 13) but cannot be screened with the anionic layers in ES-II (Figure 12b). Also, the triclinic deformation of the polymer backbone in ES-I can select the placement of chlorine ions in every second hollow of the polymer zigzag.

Another important feature is that starting from amorphous bases EB-I and EB-II, the crystallinity of polyaniline increases with the doping level. Such an effect can be explained by the fact that the insertion of Cl⁻ anions between polymer chains adds Coulomb force which makes the structure more rigid and favors the crystalline state. In this regard it is interesting to remark that by doping with HCl small crystalline regions are formed in EB-I (Figure 6) with a local structure very close to that of heavily doped materials, as shown by an only weak change in d spacings with the doping level x (Figure 5). Formation of local heavily doped regions even at very low overall doping level was previously noticed in polyacetylene doped with acceptor.[7,39] Such formation of a separated doped phase agrees with the expected reduction of elastic energy costs associated with the insertion of independent ions into the polymer. The inhomogeneous structure points to the central role of the amorphous regions ("barriers") in charge conduction, especially for intermediate doping levels.[21]

We now address the anionic sublattice of ES-I and ES-II. Both structures possess a translational symmetry of one polymer zigzag. This symmetry more likely favors electronic periodicity of c and thus the polaronic configuration (Figure 1ii). The placement of the chlorine anion in one hollow out of two will also induce an external potential on the level of one N site out of two, which c periodicity corresponds to the wave vector $4k_F$ when there is $1/2$ carrier per N (the case for $x = 0.5$). Such a potential could affect the electronic properties if the $4k_F$ charge density wave response of the polymer chain is important.[49] Such effects are observed in quasi-1D conductors with $1/2$ carrier per repeat unit like the (TMTTF)$_2$X series. However, because doped polyaniline has an intrinsic in-chain conductivity at least of the order of 10 S/cm,[21,22,24,35,50] $4k_F$ charge localization does not occur at room temperature. This anion periodicity may be the origin of the stability of the polaronic form of the ordered regions as opposed to the bipolaronic form of the disordered regions[30] and tetramer oligomers.[51] The lower conductivity of emeraldine salt at low temperature[21,22] and the lower conductivity of the polyaniline derivatives such as the poly-(o-toluidine hydrochloride) (a CH$_3$ group replacing one hydrogen of each ring)[52] reflect the presence of increased localization which is perhaps aided by the $4k_F$ potential introduced by the Cl⁻'s.

A substantial difference between ES-I and ES-II is the quite different value of the c zigzag repeat periodicity: 9.6 Å compared to 10.4 Å, respectively. Assuming a constant N–ring–N length of 5.52 Å, this leads to a sizable difference in the zigzag angles: 120° in ES-I compared to 140° in ES-II. This in principle leads to differences in the electronic properties between the two salts. Recent electron spin resonance and static susceptibility studies[53,54] in fact show some differences in the density of states in the two salts.

Another important structure parameter is the ring torsion angle ϕ. Within the crystalline EB-II the phenyl rings alternate their torsion angle by $\phi \approx \pm30°$ (ignoring the effect of the quinoid units). The structure allows room for the change of local ring angle that occurs upon photoexcitation of charges to form a positive ring torsion angle polaron.[10,13,55] (The negative polarons are expected to involve only changes in bond lengths, not changes in ϕ.[10,55])

The ring torsion decreases to a value close to zero in both salt structures. Small values of ϕ, by increasing the overlap between wavefunctions on adjacent rings, will cause increased delocalization of individual carriers along the polymer chain.[10] In this matter it is noted that the movement of charge in the polaronic fully doped ($x = 0.5$) structure is not accompanied by a change of ring angle, because all the rings of the polymer have the same electronic structure (Figure 1ii). This is not the case for the bipolaron for which there are no electrons in the bipolaron energy band and displacement of a doubly charged bipolaron implies a change of the ring electronic structure from benzenoid to quinoid (Figure 1iii). In the crystalline part of ES-I and ES-II substantial ring rotations are certainly inhibited by the compact packing of polymer chains. This packing is similar for both salt structures (same interchain distance of ca. 3.5 Å) and leads to substantial three-dimensional charge delocalization.[52]

The linear increase of spin susceptibility,[16] which accompanies the gradual increase of crystallinity of EB-I material with doping level, as well as its rapid increase in the EB-II material for doping levels $x \geq 0.25$ (i.e., after the "crystalline" EB-II becomes doped) demonstrates that the metallic regions are associated with the crystalline portion of the sample.

With increasing doping level x, the d spacings of the crystalline part of ES-I change until about $x \sim 0.2$–0.3 = x_c and then remain constant for higher doping levels (Figure 5). Only the size of individual crystalline domains still increases above x_c (Figure 6). The evolution of the lattice parameters for low doping levels is particularly remarkable. The increase of d_{001} with x can be related to an increase of the chain angle with respect to the (a,b) basal plane. The increase of d_{010} and the decrease of d_{100} and d_{110} from values close to that of EB-II for $x \sim 0$ mean that the lateral array of polymer chains evolves substantially with x. According to our structural determinations of EB-II and ES-I ($x \sim 0.5$), these changes can be correlated with the decrease of the ring tilt angle ϕ when the carrier concentration increases with x. These structural features, which lead to a decrease of the interchain interactions for x smaller than x_c, can be associated with the rapid drop of the transverse diffusion coefficient of the carriers observed below x_c by resonance methods.[24,56]

Regardless of the type of preparation, ca. 50% of the polyaniline base cannot be transformed by doping into "crytalline" salt. Both ES-I and ES-II are ca. 50% amorphous even in the fully doped state. In these amorphous parts the polymer chain conformation is probably strongly affected by defects (chain bends, chain twists, etc.). These regions remain spinless upon protonation[30] and form less conducting barriers between conducting regions.[21]

The domain length L given in Tables I–III as deduced from eq 2 applied to the fwhm of the reflections at small θ angle assumes that the polymer is composed of crystallites of finite size. This analysis gives domain sizes in the emeraldine base EB-II comparable to that previously determined for the polyacetylene, prepared by the Shirakawa method, both in transverse direction ($L_\perp \sim$ 50–100 Å compared to 80 Å in (CH)$_x$[39]). The largest values of $L_\perp$, ca. 100 Å, are observed in the emeraldine base obtained by evaporation of the THF-extracted solution. Extracted samples are composed of shorter polymer chains which can be ordered laterally more easily. Fully doped ES-I and ES-II have $L_\perp$ values comparable to that of EB-II. For ES-I $L_\parallel \sim L_\perp$. These domain sizes are ca. 2 times larger than those reported in CH$_x$ doped with anions like

I_3^- [39] or ClO_4^-.[7] This could be due to the fact that with ionic volume smaller, Cl^- can penetrate more easily between polymer chains. $L_\parallel$ and $L_\perp$ decrease significantly with decreasing x in ES-I.

It should be noted that the domain size values L given in Tables I–III are in fact lower limits of the crystalline domain size because generally several reflections are superimposed in a Debye–Scherrer ring, making it appear broader. In addition, as previously shown for polyacetylene,[57] the Scherrer formula assumes a clear-cut separation between ordered and disordered regions in the polymer. A more complete description must take into account a more gradual loss of order by conformational disorders in the chain direction, fluctuations of interchain distances, ring tilt defects, irregularities in the placement of the dopant, etc. Despite the crudeness of the picture of the order/disorder assumed for the Scherrer formula, it is interesting to realize that in emeraldine salt the crystalline domain size of ca. 50 Å is comparable to the size of metallic islands of heavily doped polyaniline, deduced from the analysis of the polymer conductivity.[21,58]

6. Conclusions

We have carried out a full study of the "crystalline" component of the ES-I, EB-II, and ES-II polyaniline forms. EB-II has a structure similar to other ring-containing polymers such as poly(p-phenylene sulfide) and poly(p-phenylene oxide). A unique feature is the difference in ordering and compactness of two salt structures—ES-I and ES-II. It reflects the influence of preparation procedures on the final crystalline structure. This difference in structure has subtle effects on the electronic properties of doped polyaniline. Judging by the similarity of the Debye–Scherrer patterns, polyaniline prepared as salt and redoped with other anions such as ClO_4^- or HSO_4^- [29] adopts structures similar to the ES-I structure. Further studies are in progress[59] in order to determine the evolution of the ES-I structure with the changes in polymerization conditions and the change in polymer itself (addition of side groups etc.) and how this modifies the electronic properties. The question of how the disorder is introduced into the "crystalline" regions requires special attention.

The variation of the crystallinity and the coherence length both parallel and perpendicular to the chain direction and the interchain separation play central roles in the competition between localization of the electronic charge to a single chain and delocalization of the charge within the three-dimensional crystalline regions.

We have also determined several structural parameters of the polymer chain like the ring torsion angle ϕ and the ring–N–ring zigzag angle which can affect the electronic structure and modify physical properties of the polyaniline. The electrostatic potential of the anion sublattice and its steric effects on the polyaniline chain can also influence these properties. These findings can serve as a basis for semiempirical calculations of the electronic properties of the polyaniline chain.

References and Notes

(1) See, for example, Proceedings of the International Conference on Synthetic Metals, Kyoto, Japan, June 1986 (*Synth. Met.*

1987, 17–19), and Sante Fe, NM, June 1988 (*Synth. Met.* 1989, 27–29).
(2) Rice, M. J. *Phys. Lett.* 1979, 71A, 152.
(3) Su, W. P.; Schrieffer, J. R.; Heeger, A. J. *Phys. Rev. Lett.* 1979, 42, 1678.
(4) Brazovskii, S. A.; Kirova, N. *Pis'ma Zh. Eksp. Teor. Fiz.* 1981, 33, 6 (*JETP Lett.* 1981 33, 4). Campbell, D. K.; Bishop, A. R. *Phys. Rev. B* 1981, 24, 4859.
(5) Brazovskii, S. A. *Zh. Eksp. Teor. Fiz.* 1980, 78, 677 (*Sov. Phys. JETP* 1980, 46, 342.
(6) Baughman, R. H.; Hsu, S. L.; Pez, G. P.; Signorelli, A. J. *J. Chem. Phys.* 1978, 68, 5404.
(7) Pouget, J. P.; Pouxviel, J. C.; Robin, P.; Comes, R.; Begin, D.; Billaud, D.; Feldblum, A.; Gibson, H. W.; Epstein, A. J. *Mol. Cryst. Liq. Cryst.* 1985, 117, 75. Pouget, J. P.; Robin, P.; Comes, R.; Gibson, H. W.; Epstein, A. J.; Billaud, D. *Physica* 1984, 127B, 158.
(8) Winokur, M.; Moon, Y. B.; Heeger, A. J.; Barker, J.; Bott, D. C.; Shirakawa, H. *Phys. Rev. Lett.* 1987, 58, 2329.
(9) Boudreaux, P. S.; Chance, R. R.; Wolf, J. F.; Shacklette, L. W.; Bredas, J. L.; Themans, B.; Andre, J. M.; Silbey, R. *J. Chem. Phys.* 1986, 85, 4584.
(10) Ginder, J. M.; Epstein, A. J.; MacDiarmid, A. G. *Solid State Commun.* 1989, 72, 967. Ginder, J. M.; Epstein, A. J. *Phys. Rev. B* 1990, 41, 10674.
(11) Stafstrom, S.; Bredas, J. L.; Epstein, A. J.; Woo, H. S.; Tanner, D. B.; Huang, W. S.; MacDiarmid, A. G. *Phys. Rev. Lett.* 1987, 59, 1464.
(12) Rice, M. J.; Mele, E. J. *Phys. Rev. Lett.* 1982, 49, 145.
(13) McCall, R. P.; Ginder, J. M.; Roe, M. G.; Asturias, G. E.; Scherr, E. M.; MacDiarmid, A. G.; Epstein, A. J. *Phys. Rev. B* 1989, 39, 10174.
(14) Chiang, J. C.; MacDiarmid, A. G. *Synth. Met.* 1986, 13, 193.
(15) Epstein, A. J.; Ginder, J. M.; Zuo, F.; Bigelow, R. W.; Woo, H. S.; Tanner, D. B.; Richter, A. F.; Huang, W. S.; MacDiarmid, A. G. *Synth. Met.* 1987, 18, 303.
(16) Ginder, J. M.; Richter, A. F.; MacDiarmid, A. G.; Epstein, A. J. *Solid State Commun.* 1987, 63, 97; *Bull. Am. Phys. Soc.* 1986, 31, 582.
(17) Choi, H. Y.; Mele, E. J. *Phys. Rev. Lett.* 1987, 59, 2188.
(18) Roe, M. G.; Ginder, J. M.; Wigen, P. E.; Epstein, A. J.; Angelopoulos, M.; MacDiarmid, A. G. *Phys. Rev. Lett.* 1988, 60, 2789.
(19) Kuzmany, H.; Sariciftci, N. S.; Neugebauer, H.; Neckel, A. *Phys. Rev. Lett.* 1988, 60, 212.
(20) Shacklette, L. W.; Wolf, J. F.; Gould, S.; Baughman, R. H. *J. Chem. Phys.* 1988, 88, 3955.
(21) Zuo, F.; Angelopoulos, M.; MacDiarmid, A. G.; Epstein, A. J. *Phys. Rev. B* 1987, 36, 3475.
(22) Javadi, H. H. S.; Cromack, K. R.; MacDiarmid, A. G.; Epstein, A. J. *Phys. Rev. B* 1989, 39, 3579.
(23) Wudl, F.; Angus, R. O., Jr.; Lu, F. L.; Allemand, P. M.; Vachon, D. J.; Nowak, M.; Liu, Z. X.; Heeger, A. J. *J. Am. Chem. Soc.* 1987, 109, 3677.
(24) Nechtschein, M.; Genoud, F.; Menardo, C.; Mizoguchi, K.; Travers, J. P.; Villeret, B. *Synth. Met.* 1989, 29, E211.
(25) Monkman, A. P.; Bloor, D.; Stevens, G. C.; Stevens, J. C. H.; Wilson, P. *Synth. Met.* 1989, 29, E277.
(26) Kaya, M.; Kitani, A.; Sasaki, K. *Chem. Lett (Jpn.)* 1987, 147.
(27) Baughman, R. H.; Wolf, J. F.; Eckhardt, H.; Shacklette, L. W. *Synth. Met.* 1988, 25, 121.
(28) Fosong, W.; Jinsong, T.; Lixiang, W.; Hongfang, Z.; Zhishen, M. *Mol. Cryst. Liq. Cryst.* 1988, 160, 175.
(29) Moon, Y. B.; Cao, Y.; Smith, P.; Heeger, A. J. *Polym. Commun.* 1989, 30, 196.
(30) Józefowicz, M. E.; Laversanne, R.; Javadi, H. H. S.; Epstein, A. J.; Pouget, J. P.; Tang, X.; MacDiarmid, A. G. *Phys. Rev. B* 1989, 39, 12958.
(31) MacDiarmid, A. G.; Chiang, J. C.; Richter, A. F.; Somasiri, N. L. D.; Epstein, A. J. In *Conducting Polymers*; Alcacer, L., Ed.; D. Reidel Publishing Co.: Dordrecht, The Netherlands, 1987; p 105.
(32) Angelopoulos, M.; Ray, A.; MacDiarmid, A. G.; Epstein, A. J. *Synth. Met.* 1987, 21, 21.
(33) Huang, W. S.; Humphrey, B. D.; MacDiarmid, A. G. *J. Chem. Soc., Faraday Trans. 1* 1986, 82, 2385.
(34) Angelopoulos, M.; Asturias, G. E.; Ermer, S. P.; Ray, A.; Scherr, E. M.; MacDiarmid, A. G.; Akhtar, M.; Kiss, Z.; Epstein, A. J. *Mol. Cryst. Liq. Cryst.* 1988, 160, 151.
(35) Cromack, K. R.; Józefowicz, M. E.; Ginder, J. M.; McCall, R. P.; Du, G.; Leng, J. M.; Li, C.; Epstein, A. J.; Scherr, E.; MacDiarmid, A. G. *Macromolecules*, in press.
(36) Tang, X., private communication. MacDiarmid, A. G.; Epstein, A. J. *Faraday Discuss. Chem. Soc.* 1989, 88, 317.

(37) MacDiarmid, A. G.; Chiang, J. C.; Richter, A. F.; Epstein, A. J. *Synth. Met.* **1987**, *18*, 285.

(38) Recent study of the degree of protonation of the emeraldine with HCl of varying pH shows that the average protonation level of emeraldine for intermediate pH is lower for class II than for the earlier studied class I.[37] Józefowicz, M. E.; Epstein, A. J.; Tang, X.; MacDiarmid, A. G., to be published.

(39) Robin, P.; Pouget, J. P.; Comes, R.; Gibson, H. W.; Epstein, A. J. *Polymer* **1983**, *24*, 1558.

(40) Guinier, A. *Theorie et Technique de la Radio-crystallographie*; Dunod: Paris, 1950.

(41) Tabor, B. J.; Magre, E. P.; Boon, J. *Eur. Polym. J.* **1971**, *7*, 1127.

(42) Boon, J.; Magre, E. P. *Makromol. Chem.* **1969**, *126*, 130.

(43) *International Tables for Crystallography: Space Group Symmetry*; Hahn, T., Ed.; D. Reidel Publishing Co.: Dordrecht, The Netherlands, 1983; Vol. A.

(44) Richter, A. F.; Ray, A.; Ramanathan, K. V.; Manohar, S. K.; Furst, G. T.; Opella, S. J.; MacDiarmid, A. G.; Epstein, A. J. *Synth. Met.* **1989**, *29*, E243.

(45) Asturias, G. E.; MacDiarmid, A. G.; McCall, R. P.; Epstein, A. J. *Synth. Met.* **1989**, *29*, E157.

(46) Pauling, L. *The Nature of the Chemical Bond*, 3rd ed.; Cornell University Press: Ithaca, NY, 1973.

(47) This corrects our previous indexing from ref 30.

(48) Baughman, R. H.; Murthy, N. S.; Miller, G. G. *J. Chem. Phys.* **1983**, *79*, 515.

(49) Emery, V. J.; Bruinsma, R.; Barisic, S. *Phys. Rev. Lett.* **1982**, *48*, 1039.

(50) Theophilou, N.; MacDiarmid, A. G.; Djurado, D.; Fischer, J. E.; Epstein, A. J. *Solid State Sci.* **1989**, *91*, 29.

(51) Javadi, H. H. S.; Treat, S. P.; Ginder, J. M.; Wolf, J. F.; Epstein, A. J. *J. Phys. Chem. Solids* **1990**, *51*, 107.

(52) Wang, Z. H.; Javadi, H. H. S.; Ray, A.; MacDiarmid, A. G.; Epstein, A. J. *Phys. Rev. B* **1990**, *42*, 5411.

(53) Laversanne, R.; Javadi, H. H. S.; Vaca-Segonds, P.; Narayan, K. S.; Epstein, A. J.; Kohli, R. K.; Scherr, E. M.; MacDiarmid, A. G., to be published.

(54) Vaca-Segonds, P.; Józefowicz, M. E.; Narayan, K. S.; Epstein, A. J.; Tang, X.; MacDiarmid, A. G., to be published.

(55) McCall, R. P.; Ginder, J. M.; Leng, J. M.; Ye, H. J.; Manohar, S. K.; Masters, J. G.; Asturias, G. E.; MacDiarmid, A. G.; Epstein, A. J. *Phys. Rev. B* **1990**, *41*, 5202.

(56) Mizoguchi, K.; Nechtschein, M.; Travers, J. P.; Menardo, C. *Synth. Met.* **1989**, *29*, E417. Mizoguchi, K.; Nechtschein, M.; Travers, J. P.; Menardo, C. *Phys. Rev. Lett.* **1989**, *63*, 66.

(57) Pouget, J. P. In *Electronic Properties of Polymers and Related Compounds*; *Springer Ser. Solid State Sci.* **1985**, *63*, 26.

(58) Wang, Z. H.; Cromack, K.; Scherr, E.; MacDiarmid, A. G.; Epstein, A. J., to be published.

(59) Józefowicz, M. E.; Epstein, A. J.; Pouget, J. P.; Masters, J. G.; Ray, A.; Sun, Y.; Tang, X.; MacDiarmid, A. G. *Synth. Met.*, in press and to be published.

(60) In contrast with these results it has been observed recently that some unstretched films of class II materials can be nearly completely amorphous in both their base and salt forms (Laridjani, M.; Pouget, J. P.; Epstein, A. J.; et al., to be published). The nature of the preparation and processing parameters controlling the degree of crystallinity in EB-II and ES-II unstretched films is under investigation.

Registry No. Polyaniline, 25233-30-1.